

# Cyclic Loading Test for Reinforced Concrete Frame with Thin Steel Infill Plate

In-Rak Choi<sup>1</sup> and Hong-Gun Park<sup>2</sup>

**Abstract:** An experimental study was performed to investigate the cyclic behavior of walls that are composed of reinforced concrete boundary frames and thin steel infill plates. For this purpose, three-story steel plate infilled walls (SPIW) were tested. The parameters in this test were the reinforcement ratio of the columns and opening in the infill plates. A reinforced concrete infilled wall (RCIW) and a reinforced concrete frame (RCF) were also tested for comparison. The deformation capacity of the SPIW specimens was significantly greater than that of the RCIW specimen, though the specimens exhibited an identical load-carrying capacity. Similar to the steel plate walls with steel boundary frames, the SPIW specimens showed excellent strength, deformation capacity, and energy dissipation capacity. Furthermore, by using the steel infill plates, shear cracking and failure of the column-beam joints were prevented. By using the strip model, the strength and initial stiffness of the SPIW specimens were predicted. The prediction results were compared with the test results. DOI: 10.1061/(ASCE)ST.1943-541X.0000317. © 2011 American Society of Civil Engineers.

**CE Database subject headings:** Steel plates; Shear walls; Reinforced concrete; Frames; Cyclic tests.

**Author keywords:** Steel plates; Shear walls; Reinforced concrete; Frames; Cyclic tests.

## Introduction

Reinforced concrete walls and steel-braced frames have been used as the primary lateral-load resisting systems for building structures. However, steel plate walls can be considered as substitutes for traditional lateral-load resisting systems. In particular, they can be used for enhancing earthquake resistance. The steel plate wall consists of a boundary frame and infill plates that are welded or connected by bolts to the boundary frame. Recently, to increase convenience in construction and decrease costs, steel plate walls with unstiffened thin infill plates have been studied by many researchers (Thorburn et al. 1983; Caccese et al. 1993; Driver et al. 1998; Elgaaly 1998; Lubell et al. 2000; Berman and Bruneau 2003; Park et al. 2007; Choi and Park 2008). According to their studies, the steel plate walls with unstiffened thin infill plates have good ductility and energy dissipation capacities as well as high strength. In particular, when the boundary columns have sufficient strength to resist the tension field forces of the infill plates, yielding of the infill plates is distributed along the building height. Therefore, when such walls are used for low-rise or medium-rise buildings, they can show shear-dominated behavior and have excellent ductility and energy dissipation capacities [Fig. 1(a)].

On the other hand, conventional reinforced concrete walls, which have a concentrated plastic hinge at the bottom, exhibit cantilever flexural behavior [Fig. 1(b)]. Because the overall inelastic

deformation is governed by the plastic deformation of the single plastic hinge, the ductility and energy dissipation of reinforced concrete walls cannot be increased to levels as high as those of the steel plate walls. Furthermore, reinforced concrete walls with thin infill concrete panels are susceptible to brittle crushing failure of the concrete subjected to shear. In this case, by replacing conventional infill concrete panels with thin steel plates, the ductility of the wall can be significantly increased by showing shear-dominated behavior [Fig. 1(a)] and preventing early crushing of concrete. In addition to the structural advantage, various advantages are expected, in which thin steel plates are used to strengthen new or existing reinforced concrete structures. The overall weight of a structure can be reduced by using thin steel plates. Faster construction is enabled by reducing concrete form work and concrete curing. Furthermore, it is easy to relocate or penetrate existing walls, according to continuous changes in function of the room (Baldelli 1983).

In the present study, to enhance the ductility and energy dissipation capacities of concrete structures, a wall system that consists of a reinforced concrete boundary frame and thin steel infill plates was investigated. The steel infill plates were used to replace conventional infill concrete panels. By using steel infill plates, the walls were designed to exhibit the shear-dominated behavior, as shown in Fig. 1(a). The steel plate infilled walls (SPIWs) were tested for cyclic loading. For comparison, an RCF with concrete infill panels was tested.

## Specimens and Test Setup

The test specimens were designed as one-third-scale models of three-story prototype walls with steel infill plates. The properties of the test specimens are listed in Table 1. The dimensions and reinforcement details of the specimens are shown in Fig. 2. The specimens SPIW1 and SPIW2 were designed as steel plate infilled walls. In typical buildings, frequently, windows, doors, and corridors are located in the walls. To investigate the effect of wall opening on the structural capacity, specimen SPIW3 having an opening in the web was tested. A reinforced concrete infilled wall (RCIW)

<sup>1</sup>Senior Researcher, Research Institute of Industrial Science and Technology, POSCO Global R&D Center, 180-1 Songdo-Dong, Yeosu-Gu, Incheon 406-840, South Korea. E-mail: irchoi@rist.re.kr

<sup>2</sup>Professor, Dept. of Architecture, Seoul National Univ., San 56-1, Shinlim-Dong, Kwanak-Gu, Seoul 151-744, South Korea (corresponding author). E-mail: parkhg@snu.ac.kr

Note. This manuscript was submitted on July 7, 2009; approved on September 12, 2010; published online on September 22, 2010. Discussion period open until November 1, 2011; separate discussions must be submitted for individual papers. This paper is part of the *Journal of Structural Engineering*, Vol. 137, No. 6, June 1, 2011. ©ASCE, ISSN 0733-9445/2011/6-654-664/\$25.00.

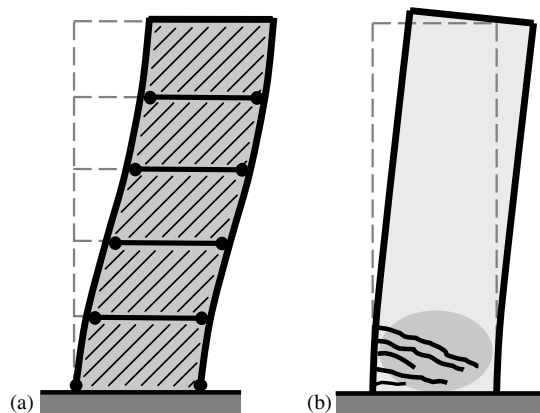


**Fig. 1.** Comparison of inelastic deformation modes: (a) shear mode of the steel plate walls with thin steel plates; (b) cantilever flexure mode of reinforced concrete walls

and a reinforced concrete moment frame (RCF) were also tested to verify the structural capacity of the SPIWs by comparing the structural capacities. The RCIW was designed as a special reinforced concrete wall in accordance to building code requirements ACI 318-08 [American Concrete Institute (ACI) 2008], with the same design strength as the SPIW1. The RCF consisted of beams and columns that had the same dimensions and reinforcement details as those used for SPIW1. In all the specimens, the boundary frames were designed as special moment frames that conform to ACI 318-08.

The reinforcement ratios of the columns in SPIW1 and SPIW2 were 3.7% and 5.1%, respectively. The thickness of the steel infill plates in both specimens was 2 mm (Korean Standard SS400,  $F_y = 240$  MPa), and their aspect ratio ( $l_p/h_p$ ) was 1.5 ( $l_p = 1,500$  mm and  $h_p = 1,000$  mm, where  $l_p$  and  $h_p$  are the length and height of the steel infill plate, respectively). The thickness and aspect ratio of the steel infill plates are the same as those used for the steel plate wall specimen SC2T that Park et al. (2007) tested.

In SPIW3, as shown in Fig. 2(b), the infill plates had an opening with a length of 600 mm. The infill plates were connected by coupling beams at the openings. For cost-saving, end plates (SS400, width = 100 mm, thickness = 12 mm) were welded to

the free edges of the steel plates, instead of using boundary columns (Fig. 2). The thickness of the infill plates in SPIW3 was 4 mm (SS400).

The dimensions and reinforcement details of the boundary frame members are shown in Fig. 2. The cross sections of the columns, beams, and top beams were  $300 \times 300$  mm,  $300 \times 200$  mm, and  $300 \times 300$  mm, respectively. To ensure the development of a shear-dominated deformation mode [Fig. 1(a)], the columns in the steel plate infilled walls were designed to have sufficient strengths for resisting the tension field forces of the steel infill plates. According to Park et al. (2007), assuming that the tension field forces are uniformly distributed along the column length and fixed end condition, the axial force ( $P_u$ ), bending moment ( $M_u$ ), and shear force ( $V_u$ ) acting on a column can be approximately estimated as

$$P_u = n_s h_s F_y t \sin \alpha \cos \alpha \quad (1)$$

$$M_u = \frac{1}{12} R_y F_y t h_s^2 \sin^2 \alpha \quad (2)$$

$$V_u = \frac{1}{2} R_y F_y t h_s \sin^2 \alpha \quad (3)$$

where  $n_s$  = number of stories;  $h_s$  = story height;  $R_y$  = overstrength factor for the steel infill plate (= 1.3 for SS400 steel);  $F_y$  and  $t$  = design yield strength and thickness of the steel infill plate, respectively; and  $\alpha$  = inclination angle of the tension field ( $\alpha$  is assumed to be  $45^\circ$  for preliminary design).

To transfer the forces between the steel infill plates and RCF, as shown in Fig. 2(d), studs were embedded in the columns and beams. The design forces for the studs were estimated by assuming that the tension field forces of the steel plate were uniformly distributed along the boundary frame. Then, the number of studs and the size of end plate were determined according to Precast/Prestressed Concrete Institute (PCI) (1999). In the design, the concrete compressive strength was assumed to be 26 MPa, and the yield stress of the studs was 240 MPa. Two rows of studs (diameter = 13 mm, length = 150 mm) were welded to the end plates (width = 100 mm, thickness = 12 mm) at intervals of 100 mm. The steel infill plates were weld-connected to the end plates by fish plates that were 50-mm wide and 6-mm thick (SS400) [Fig. 2(d)].

**Table 1.** Properties of Test Specimens

		SPIW1 (steel plate infilled wall)	SPIW2 (steel plate infilled wall)	SPIW3 (steel plate infilled wall with an opening)	RCIW (RC infilled wall)	RCF (RC frame)	
Concrete compressive strength, MPa		26.4	26.4	26.4	32.1	26.4	
Infilled steel plate	Thickness (mm)	2	2	4	—	—	
	Yield strength (MPa)	302	302	300	—	—	
Infill RC panel	Horizontal reinforcement <sup>a</sup>	—	—	—	0.65	—	
	Vertical reinforcement <sup>a</sup>	—	—	—	0.43	—	
Column	Longitudinal reinforcement	3,336 <sup>b</sup>	4,596 <sup>c</sup>	3,336 <sup>b</sup>	3,097 <sup>d</sup>	3,336 <sup>b</sup>	
		Reinforcement ratio (%)	3.7	5.1	3.7	3.4	3.7
	Transverse reinforcement <sup>a</sup>	Spacing (mm)	50	50	50	50	50
Beam	Longitudinal reinforcement	794 <sup>e</sup>	794 <sup>e</sup>	794 <sup>e</sup>	794 <sup>e</sup>	794 <sup>e</sup>	
		Reinforcement ratio (%)	1.3	1.3	1.3	1.3	1.3
	Transverse reinforcement <sup>a</sup>	Spacing (mm)	60	60	Midspan: 50 Both ends: 60	60	60

<sup>a</sup>D10 ( $A_b = 71.3$  mm<sup>2</sup>,  $f_y = 486$  MPa).

<sup>b</sup>6-D22 ( $A_b = 387.1$  mm<sup>2</sup>,  $f_y = 430$  MPa) and 2-D25 ( $A_b = 506.7$  mm<sup>2</sup>,  $f_y = 443$  MPa).

<sup>c</sup>4-D25 ( $A_b = 506.7$  mm<sup>2</sup>,  $f_y = 443$  MPa) and 4-D29 ( $A_b = 642.4$  mm<sup>2</sup>,  $f_y = 486$  MPa).

<sup>d</sup>8-D22 ( $A_b = 387.1$  mm<sup>2</sup>,  $f_y = 430$  MPa).

<sup>e</sup>4-D16 ( $A_b = 198.6$  mm<sup>2</sup>,  $f_y = 471$  MPa).

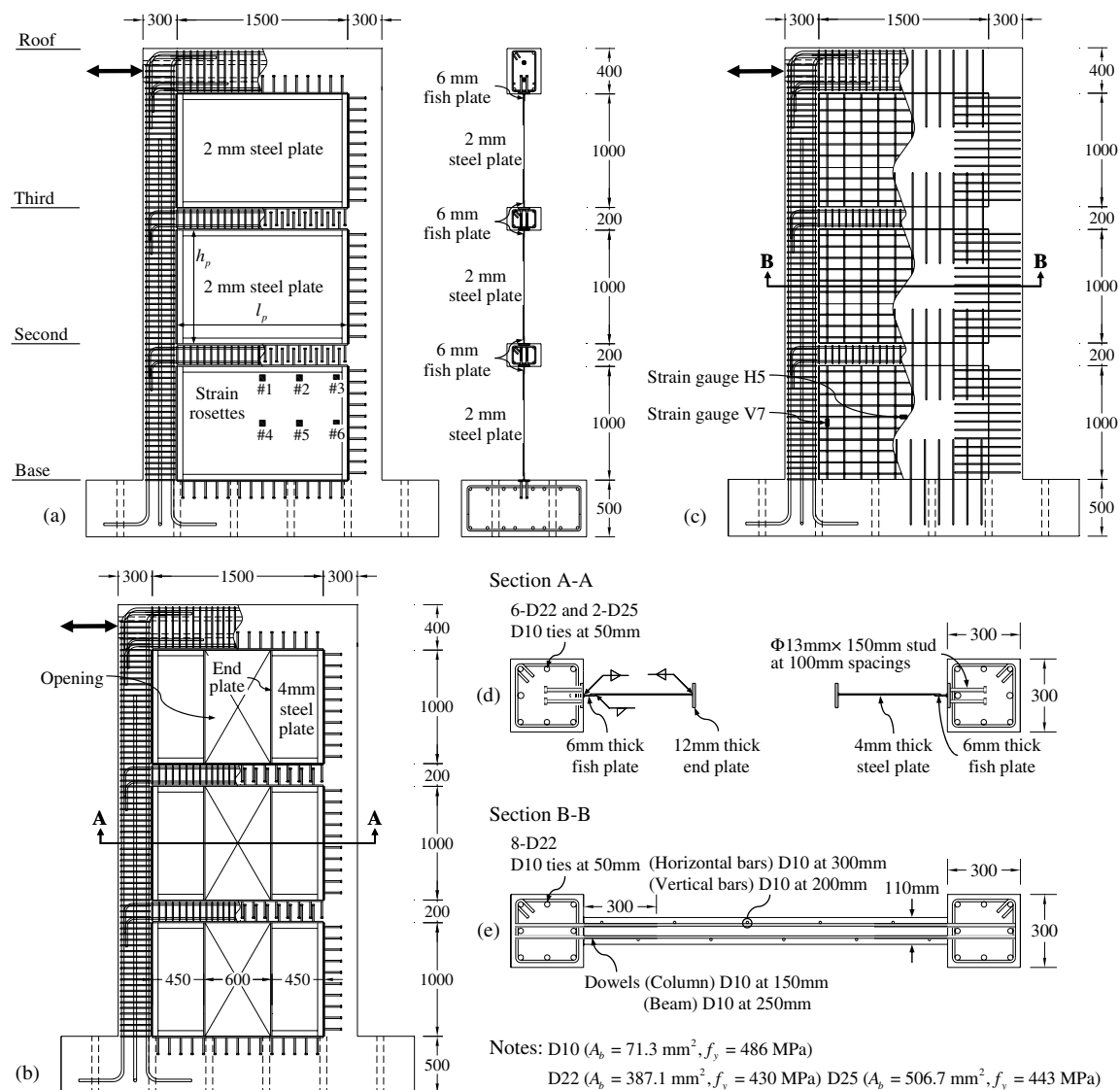


**Fig. 2.** Dimensions and reinforcement details of test specimens (mm): (a) SPIW1; (b) SPIW3; (c) RCIW; (d) section A-A of SPIW3; and (e) section B-B of the RCIW

In the RCIW, 110-mm-thick reinforced concrete infill panels were used instead of steel plates. The infill concrete panel was doubly reinforced. The reinforcement ratios were  $\rho_v = 0.65\%$  in the vertical direction and  $\rho_h = 0.43\%$  in the horizontal direction (Table 1). To transfer the forces between the infilled wall and boundary frame, two rows of 10-mm-diameter dowel bars were placed at intervals of 150 mm in the columns and 250 mm in the beams. The details of the reinforcement and dowels used for the RCIW are shown in Fig. 2(e).

The measured strengths of the concrete and rebars along with the average results of the coupon tests for the steel plate are listed in Table 1. The concrete strength for the RCIW was 32.1 MPa, and the concrete strength for other specimens was 26.4 MPa. The yield strength of the steel infill plates was 300 MPa and 302 MPa. The yield strength of the rebars ranged from 430 MPa to 486 MPa.

The test setup and instrumentation are shown in Fig. 3. Each specimen was laterally loaded at the top beam. No axial load was applied on the specimens. The specimens were braced at the second-, third-, and top-story beams to prevent out-of-plane displacements. During the test, lateral displacements and average shear distortions at each story were measured by potentiometer-

type displacement transducers ( $w$ -LVDTs) and diagonally placed displacement transducers (LVDTs), respectively.

The loading was controlled by the displacement at the top beam. The yield displacement  $\delta_y$  at the top of the steel plate infilled walls was estimated by numerical analysis to be 15 mm. On the basis of the yield displacement  $\delta_y$  ( $= 15$  mm), the target displacements for the cyclic loading were set as  $\pm 0.2\delta_y$ ,  $0.4\delta_y$ ,  $0.6\delta_y$ ,  $0.8\delta_y$ ,  $1.0\delta_y$ ,  $1.5\delta_y$ ,  $2\delta_y$ ,  $3\delta_y$ ,  $4\delta_y$ ,  $6\delta_y$ , and  $8\delta_y$ . Cyclic loadings were repeated three times at each target displacement. The loading history was the same as that used for the steel plate walls tested by Park et al. (2007) and Choi and Park (2008, 2009).

## Test Results

### Load-Story Drift Ratio Relationship

Fig. 4 shows the load-average story drift ratio relationships obtained from the test. Fig. 4(f) compares the envelope curves of the load-average story drift ratio relationships for all the specimens. The average story drift ratio was calculated by the top lateral dis-

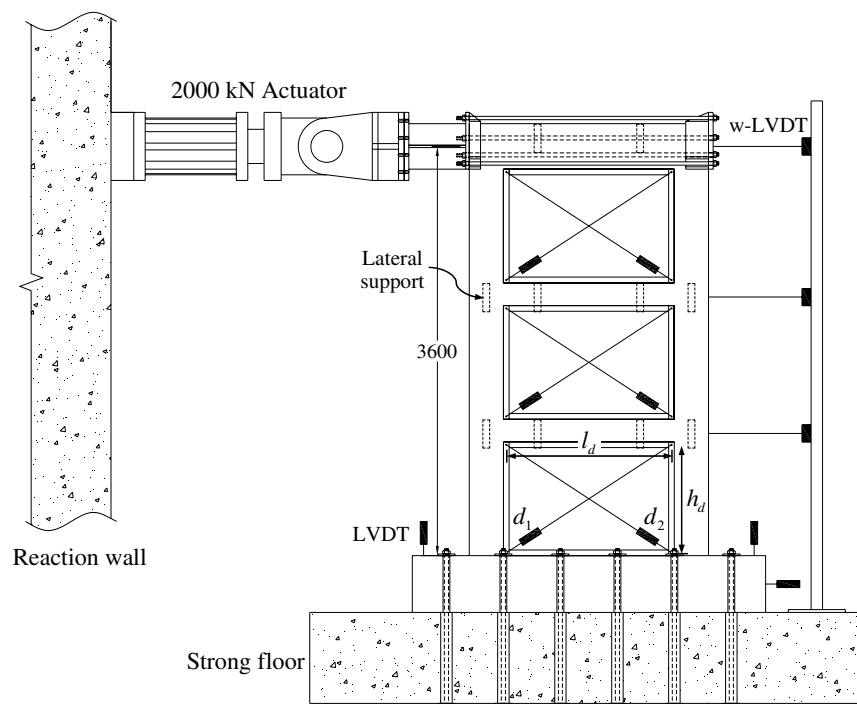


Fig. 3. Test setup and instrumentation

placement divided by the wall height. The test results at the yield point, maximum load, and maximum displacement of the specimens are summarized in Table 2. The definition of the yield point ( $\delta_y, P_y$ ) was on the basis of the concept of equal plastic energy such that the area enclosed by the idealized elastoplastic envelope curve was equal to that enclosed by the actual envelope curve [see Fig. 4 (f)]. For the specimens that show softening behavior after peak loading, the maximum displacement (or deformation capacity  $\delta_{max}$ ) was defined as the postpeak displacement corresponding to 80% of the maximum load.

As shown in Fig. 4 and Table 2, the steel plate infilled walls SPIW1 and SPIW2 exhibited large initial stiffness, load-carrying capacities, and deformation capacities. Although the reinforcement ratio of the columns in SPIW2 was greater than that of the columns in SPIW1 by a factor of 1.4, their load-carrying capacities and deformation capacities were not significantly different. This is because the overall behavior of both walls was governed by the yielding of the steel infill plates rather than by the strength of the boundary members. Whereas the steel plate infilled wall SPIW1 showed almost the same load-carrying capacity as the RCIW [Fig. 4(d)], its deformation capacity  $\delta_{max}$  and displacement ductility  $\delta_{max}/\delta_y$  were greater than those of the RCIW by factors of 1.3 and 1.5, respectively. The displacement ductility of SPIW1 was greater than that of the moment frame RCF [Fig. 4(e)] by a factor of 1.1.

Fig. 5 shows the results of tests performed on the steel plate wall SC2T by Park et al. (2007) in a previous study. The thickness of the infill plates in SC2T was 2 mm (SS400) and the column was  $H-250 \times 250 \times 20 \times 20$  mm [built-up wide-flange section;  $H$ -overall depth ( $d_c$ )  $\times$  flange width ( $b_f$ )  $\times$  web thickness ( $t_w$ )  $\times$  flange thickness ( $t_f$ ); area of column ( $A_c$ ) = 8,932 mm<sup>2</sup>]. The column was made of SM490 steel (Korean standard,  $F_y = 330$  MPa). The results in Figs. 4 and 5 indicate that the steel plate infilled wall SPIW with lower column strength exhibited a lower load-carrying capacity and more pinched behavior than the steel plate wall SC2T. However, there was no difference in the deformation capacity. This

result indicates that thin steel infill plates can be effectively used in the RCFs as well as the steel frames.

Figs. 4(d) and 4(e) show the results of tests performed on the RCIW and the RCF. The RCIW showed large initial stiffness and a large load-carrying capacity. However, owing to the concrete crushing in the infill concrete panel, its deformation capacity was significantly less than that of the steel plate infilled walls SPIW1 and SPIW2. The RCF exhibited a large deformation capacity. However, since the initial stiffness of the RCF was significantly low, the displacement ductility was less than that of the steel plate infilled walls SPIW1 and SPIW2. Furthermore, pinching behavior was caused by shear cracking that developed at the beam-column joints.

### Failure Mechanism

In SPIW1 and SPIW2, the local buckling and tension field action in steel plates were developed in all stories, as shown in Fig. 6(a). In SPIW1, steel plates yielded in all stories; then, plastic hinges were developed at the base of the first-story columns and at the ends of the second- and third-story beams. At an average story drift ratio of 1.7% (top displacement = 60 mm), vertical concrete cracks began to form at the first-story columns along the heads of the embedded studs [Fig. 7(b)]. At a drift ratio of 2.5% (top displacement = 90 mm), vertical concrete cracks also developed at the second-story columns. At a drift ratio of 3.3% (top displacement = 120 mm), horizontal concrete cracks developed at the second- and third-story beams where studs were embedded. During the following load cycles, fractures occurred at the welded connections between the studs and the end plates at the bottoms of the second- and third-story steel plates. Because of the fracture, the load-carrying capacity of the wall decreased. At the end of the test, the maximum out-of-plane displacement of the steel plates in the first, second, and third stories were 74, 90, and 62 mm, respectively. The failure mode and overall behavior of SPIW2 were similar to those of SPIW1.

In SPIW3, damage was concentrated at the coupling beams. At a drift ratio of 0.8% (top displacement = 30 mm), diagonal concrete

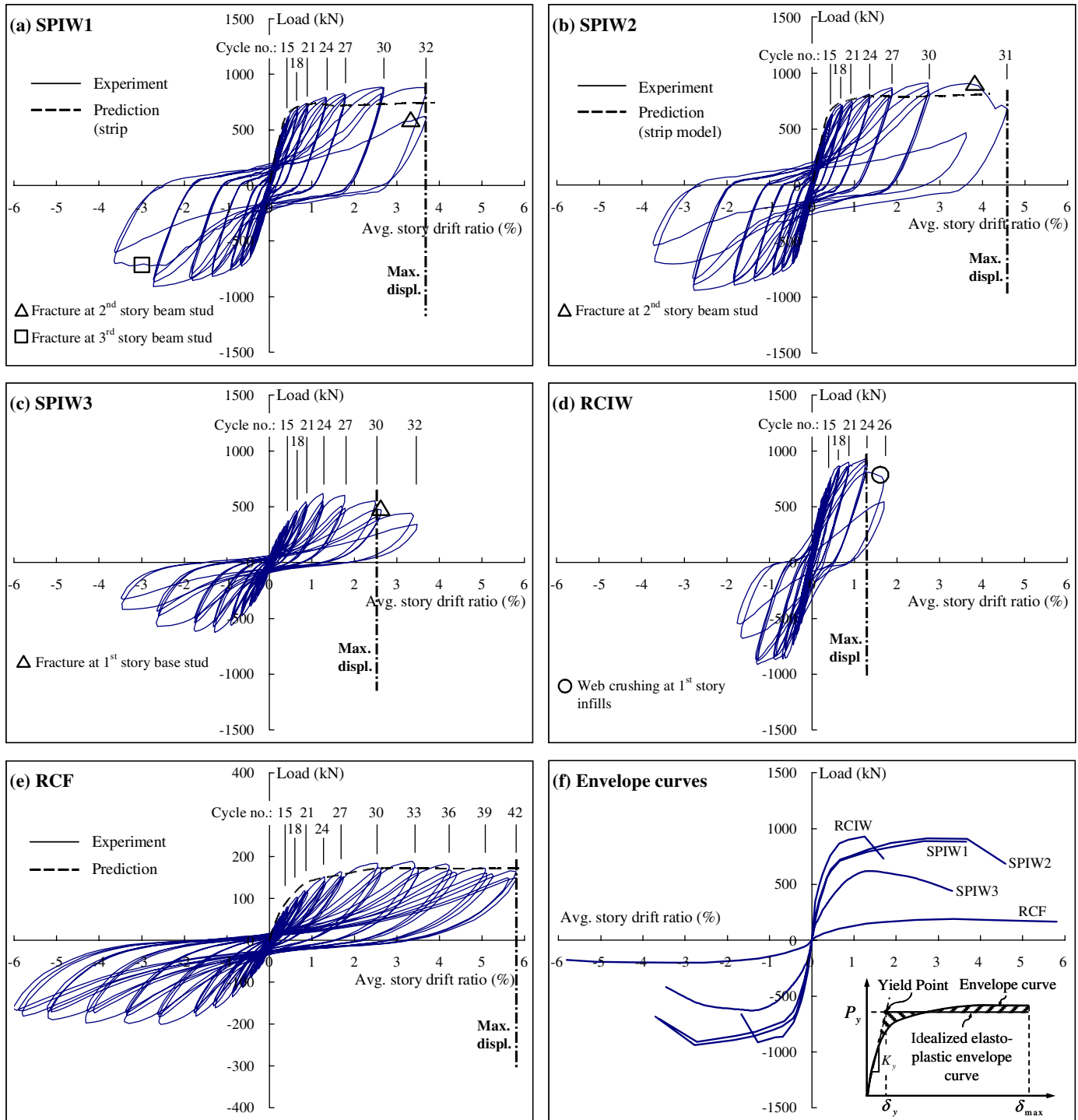


**Fig. 4.** Load-average story drift ratio relationships for test specimens

cracks were developed at the second- and third-story coupling beams. At a drift ratio of 2.5% (top displacement = 90 mm), fractures occurred at the welded connection between the studs and the end plates at the base of the end plates that were used to stiffen the boundary of the wall opening [Fig. 6(b)].

In the RCIW, unlike SPIW specimens, damage was concentrated at the first-story infill panel [Fig. 6(c)]. After 1.7% drift ratio (top displacement = 60 mm), the load-carrying capacity decreased abruptly because of the concrete crushing in the first-story infill panel.

In the moment frame RCF, plastic hinges were developed at the ends of the beams and columns. Finally, the load-carrying capacity

decreased because of the concrete crushing in the top-story column-beam joint [Fig. 6(d)].

#### Shear Distortion of Infill Panels

The average shear distortions of the test specimens were calculated from the deformations of the diagonals of each panel (Fig. 3). The average shear distortion can be calculated as follows:

$$\gamma_{\text{avg}} = \frac{\sqrt{h_d^2 + l_d^2}(d_1 - d_2)}{2h_d l_d} \quad (4)$$

**Table 2.** Test Results

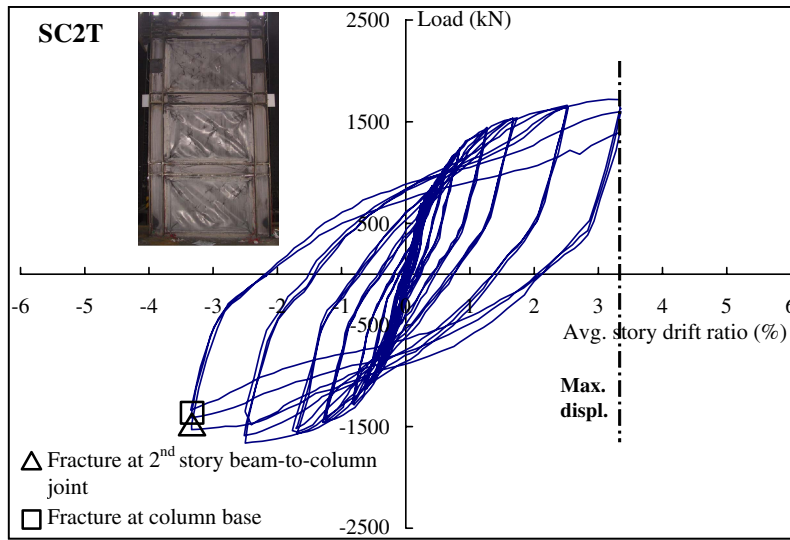
Specimen	Maximum load						Maximum displacement					
	Positive loading (+)			Negative loading (-)			Positive loading (+)			Negative loading (-)		
	$P_{max}$ (kN)	$\delta$ (mm)	Story drift <sup>a</sup> (%)	$P_{max}$ (kN)	$\delta$ (mm)	Story drift <sup>a</sup> (%)	$P$ (kN)	$\delta_{max}$ (mm)	Story drift <sup>a</sup> (%)	$P$ (kN)	$\delta_{max}$ (mm)	Story drift <sup>b</sup> (%)
SPIW1	886	95.6	2.7	-911	-98.1	2.7	882	131.6	3.7	-729	-118.4	3.3
SPIW2	914	98.2	2.7	-940	-100	2.7	795	152.4	4.2	-859	-100.3	2.8
SPIW3	618	45.7	1.3	-624	-46.1	1.3	531	90.1	2.5	-538	-95.6	2.7
RCIW	912	45.4	1.3	-913	-46.1	1.3	912	45.4	1.3	-913	-46.1	1.3
RCF	190	121.1	3.4	-200	-93.2	2.6	164	209.1	5.8	-181	-208.3	5.5

Specimen	Yield point								$P_{max}/P_y$				$\delta_{max}/\delta_y$			
	Positive loading (+)				Negative loading (-)				Positive loading		Negative loading		Positive loading		Negative loading	
	$P_y$ (kN)	$\delta_y$ (mm)	Story drift <sup>a</sup> (%)	$K_y^b$ (kN/mm)	$P_y$ (kN)	$\delta_y$ (mm)	Story drift <sup>a</sup> (%)	$K_y^b$ (kN/mm)	Positive loading	Negative loading	Positive loading	Negative loading	Positive loading	Negative loading		
SPIW1	808	15.3	0.4	53	-816	-14.5	0.4	56	1.1	1.1	8.6	8.2				
SPIW2	837	15.1	0.4	55	-850	-13.9	0.4	61	1.1	1.1	9.8	7.2				
SPIW3	547	16.9	0.5	32	-559	-14.8	0.4	38	1.1	1.1	5.3	6.5				
RCIW	843	10.4	0.3	81	-839	-12.1	0.3	69	1.1	1.1	4.4	3.8				
RCF	169	28.1	0.8	6	-181	-25.2	0.7	7	1.1	1.1	7.4	8.3				

<sup>a</sup>Maximum displacement at top divided by wall height.

<sup>b</sup>Elastic stiffness ( $K_y = P_y/\delta_y$ ).



**Fig. 5.** Load-average story drift ratio relationships for the steel plate wall SC2T (Park et al. 2007, ASCE)

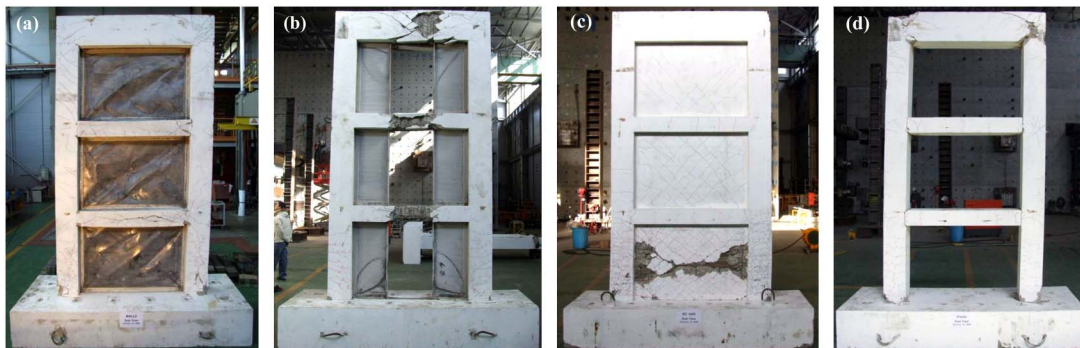


**Fig. 6.** Test specimens after failure: (a) SPIW1; (b) SPIW3; (c) RCIW; (d) RCF

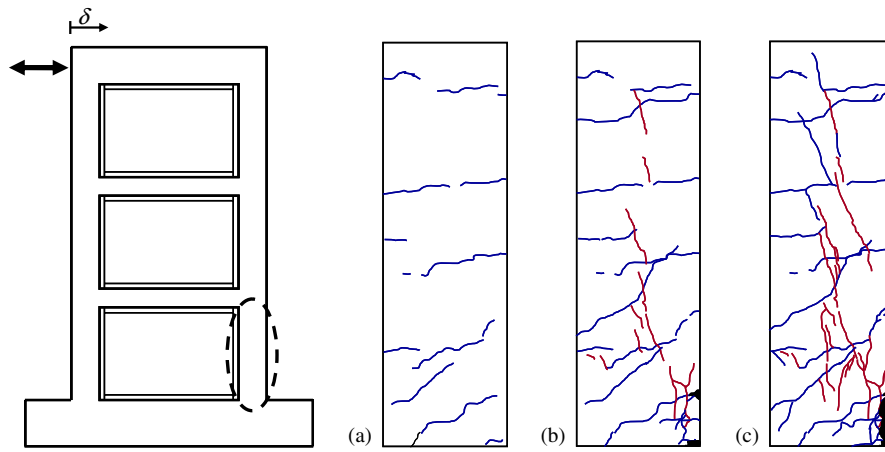


**Fig. 7.** Observed crack patterns on the first-story column in SPIW1: (a)  $\delta = 15$  mm (0.4% drift ratio); (b)  $\delta = 60$  mm (1.7% drift ratio); (c)  $\delta = 90$  mm (2.5% drift ratio)

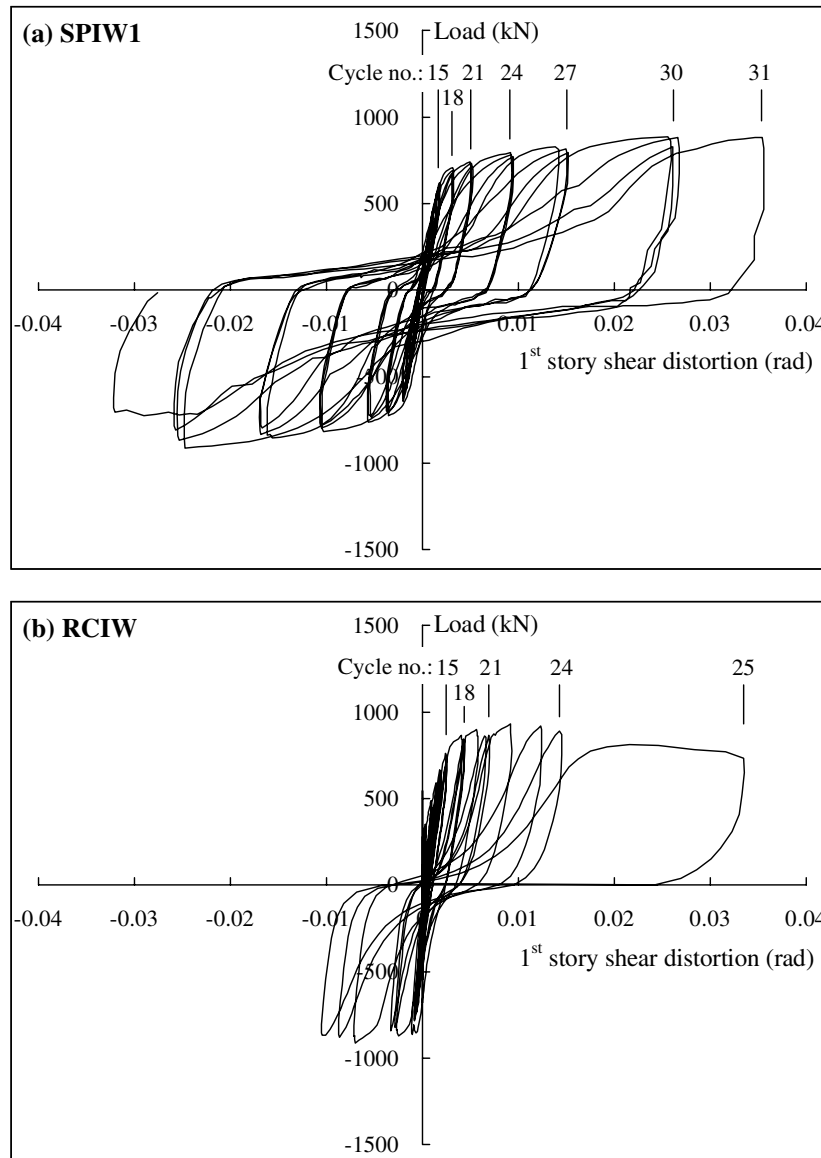


**Fig. 8.** Shear distortions at the first-story walls

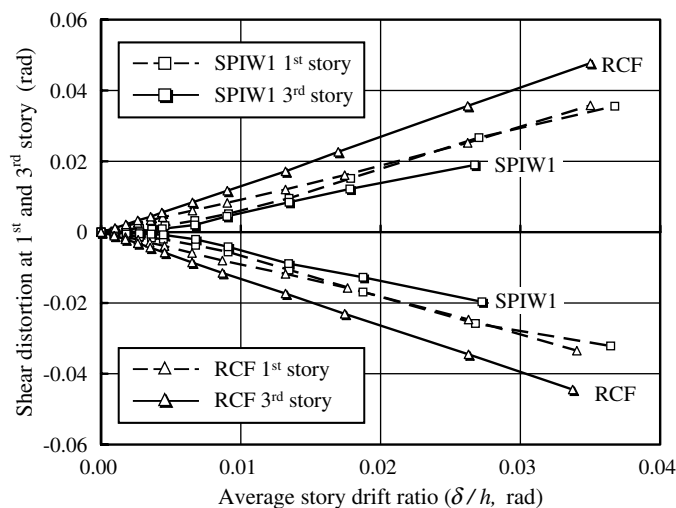


**Fig. 9.** Variations of shear distortion with the story drift ratio

where  $h_d$  and  $l_d$  = horizontal and vertical distances between the measurement points, respectively;  $d_1$  and  $d_2$  = diagonal deformations measured in each diagonal direction.

Fig. 8 shows the load-shear distortion relationships in the first story of SPIW1 and the RCIW, which were designed to have the same load-carrying capacity. As shown in Fig. 8, the RCIW showed a more pinched behavior. After load cycle 21 (0.8% drift ratio), the RCIW experienced greater shear distortion than SPIW1. The shear distortions in the positive direction were greater than those in the negative direction.

Fig. 9 shows the variations in the maximum shear distortions versus the average story drift for specimen SPIW1 and the RCF, which have the same boundary frame. In this figure, the dotted line indicates the first-story shear distortions and the solid line indicates the third-story shear distortion of each specimen. The two specimens experienced similar shear distortions at the first story. However, at the third story, the RCF exhibited twice the shear distortion that SPIW did, because of the shear cracking of the top-story beam-column joints. On the other hand, in SPIW1, shear cracking did not occur at the beam-column joints because of the strengthening effect of the steel plates.

### Strains in Infill Panels

To investigate the differences in the hysteretic behavior of the SPIW and RCIW, the measured strains in the infill panels were compared. The locations of the strain rosettes and strain gauges are shown in Figs. 2(a) and 2(c).

Fig. 10(a) shows the principal strains of the first-story steel plate in SPIW1. The principal strains are calculated from the strains measured by the strain rosettes. During early loading, local buckling of the steel plate occurred and tension field action developed. As a result, only tensile strains were measured. Yielding of the steel plates occurred at load cycle 16 (0.6% drift ratio), and then, tensile strains continuously increased during subsequent loadings.

The angle of the principal tensile strain axis indicates the inclination angle of the tension field in the steel infill plates. The angles of the principal tensile strain axis measured from the vertical direction ranged from 37° to 45° at the yield displacement of the specimens [Fig. 10(b)]. The inclination angle of the tension field ( $\alpha$ ) can be estimated by modifying the tension strip model that was proposed by Timler and Kulak (1983) for steel plate shear walls

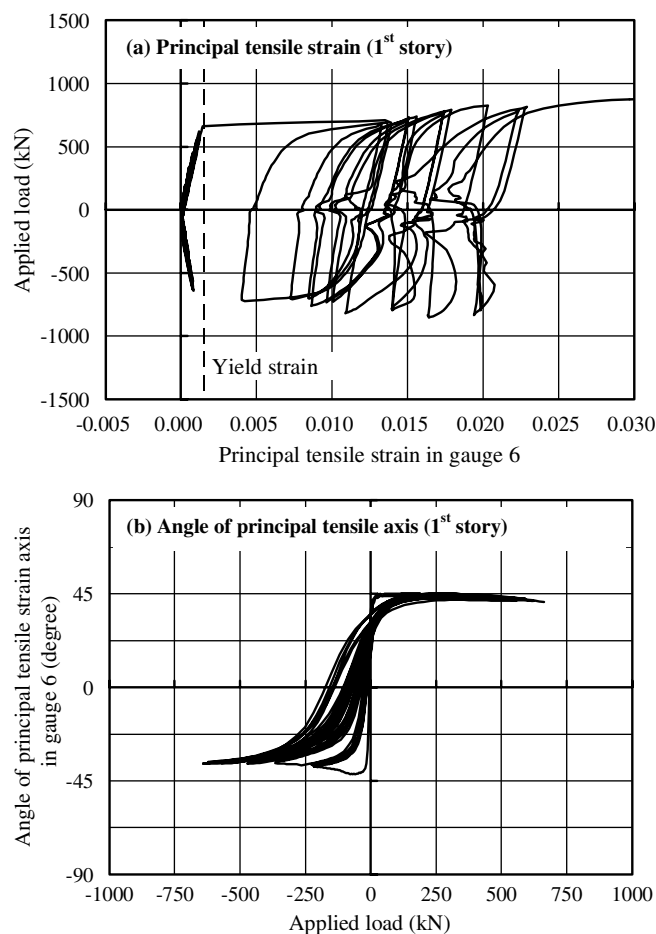


**Fig. 10.** Measured principal tensile strain and its orientation in the steel plate of the SPIW1

$$\alpha = \tan^{-1} \sqrt{\left(1 + \frac{ntl}{2A_c}\right) \left[1 + nth_s \left(\frac{1}{A_b} + \frac{h_s^3}{360I_c l}\right)\right]^{-1}} \quad (5)$$

where  $l$  = center-to-center distance between the boundary columns;  $n$  = elastic modulus ratio ( $E_s/E_c$ );  $E_s$  and  $E_c$  = elastic modulus of steel and concrete, respectively;  $A_b$  and  $A_c$  = cross-sectional areas of the beam and column, respectively; and  $I_c$  = moment of inertia of the boundary column. The inclination angle predicted by using Eq. (5) was 43°, which agrees well with the test result.

Fig. 11 shows the strains measured in the horizontal and vertical reinforcements of the infill concrete panel in the RCIW. Permanent tensile strains developed in both the vertical and horizontal bars. The maximum tensile strains of the reinforcements did not significantly exceed the yield strain, which indicates that concrete crushing failure in the infill RC panel occurred as soon as the reinforcements yielded. This result demonstrates that in reinforced concrete subjected to shear, the diagonal concrete strut is susceptible to early crushing failure when the tensile strain in the transverse direction increases.

### Energy Dissipation Capacity

The energy dissipation per load cycle is defined as the area enclosed by a hysteresis curve. The cumulative energy dissipation can be calculated by summing the energy associated with all the hysteresis loops. Fig. 12 shows the cumulative energy dissipation

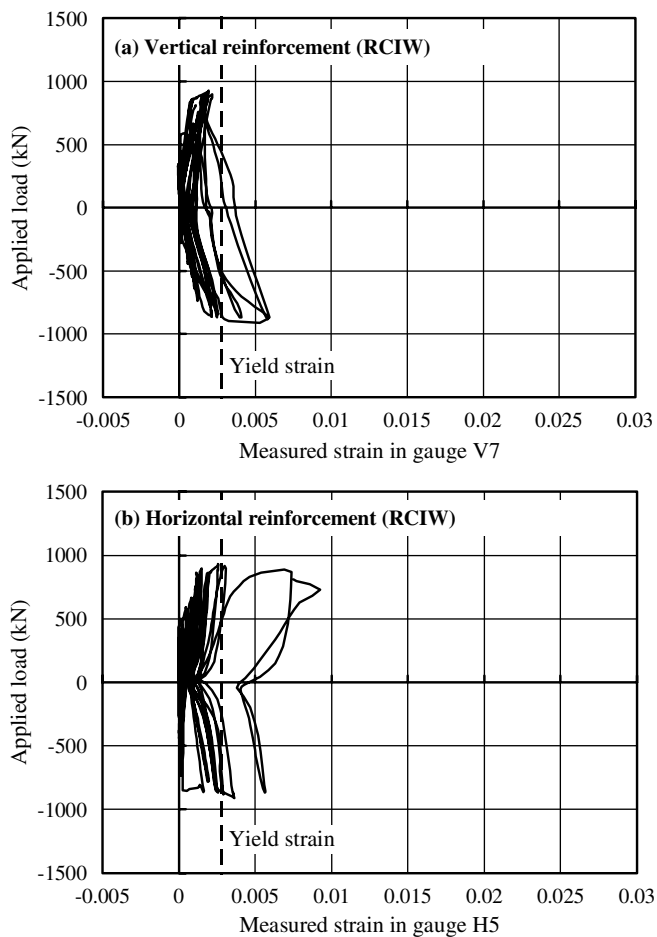


**Fig. 11.** Measured strains of the reinforcements in the infill RC panel of the RCIW

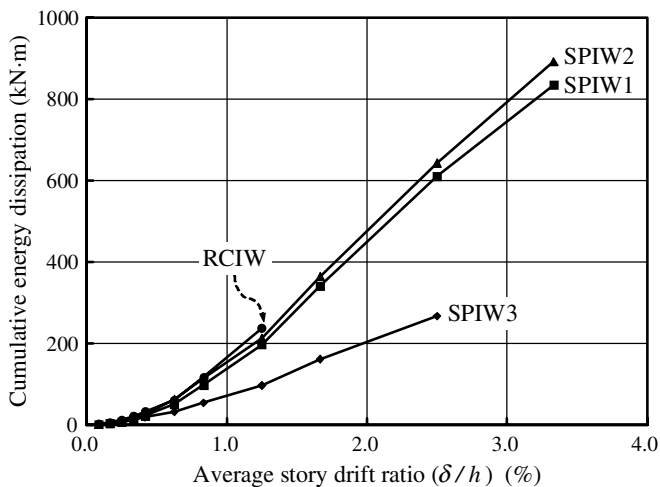


**Fig. 12.** Cumulative energy dissipation of test specimens

of the test specimens. Before concrete crushing at an average story drift ratio of 1.3% (top displacement = 45 mm), the energy dissipation capacity of the RCIW was similar to that of SPIW1. However, the total cumulative energy dissipation of SPIW1 was 3.5 times that of the RCIW. Although the columns in SPIW2 had a greater reinforcement ratio than those in SPIW1, the energy

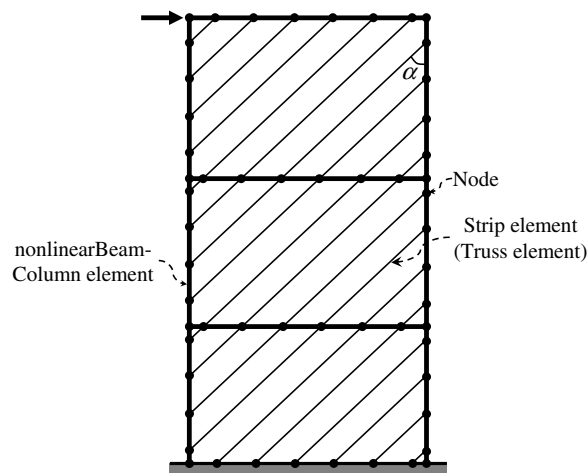


**Fig. 13.** Strip model

dissipation of SPIW2 was close to that of SPIW1. The energy dissipation of SPIW3 did not significantly increase because damage was concentrated on the coupling beams, and the steel plates did not completely yield. In SPIW1, at a drift ratio of 2.5% (top displacement = 90 mm), the ratio of the energy dissipations of the first-, second-, and third-story steel plates was 1:1.03:0.85. In SPIW2, at the same drift ratio, the corresponding ratio was 1:0.91:0.87. This result indicates that the plastic deformations of the steel infill plates were uniformly distributed along the wall height.

## Numerical Predictions

The strip model developed by Thorburn et al. (1983) has been used for the simplified analysis of steel plate shear walls with thin infill plates. In this model, thin infill plates that buckle early under cyclic shear are modeled by a series of inclined tension strips (Fig. 13).

To investigate the applicability of the strip model to the steel plate infilled walls, nonlinear push-over analysis was performed by using OpenSees (Mazzoni et al. 2006). The steel infill plates were modeled as a series of inclined pin-ended tension strips. As shown in Fig. 13, ten equally spaced tension strips were used for each panel. The inclination angle  $\alpha$  was estimated to be  $43^\circ$  by using Eq. (5). The reinforced concrete moment frames were modeled by using a nonlinear beam-column element (nonlinearBeam-Column) in OpenSees that accurately simulates the nonlinear axial-flexural behavior of RCF members. The properties determined from material tests were used for the analysis models (Table 1).

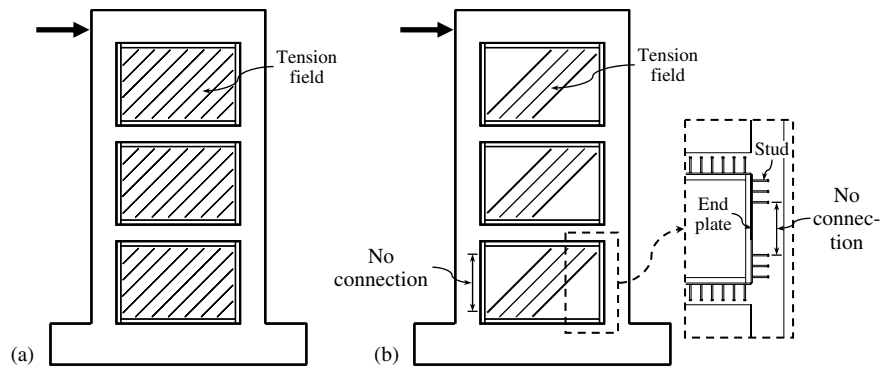
In Fig. 4, the predicted load-displacement relationships were compared with the test results for specimens SPIW1, SPIW2, and the RCF. The load-carrying capacities and initial stiffness values determined from the test and the corresponding predicted values are presented in Table 3. As shown in Fig. 4 and Table 3, the proposed strip model could be used to predict the behavior of the steel plate infilled walls with reasonable precision. However, the predicted load-carrying capacities were smaller than the actual test results because the strain-hardening effect of the steel subjected to cyclic loading was not considered.

## Discussions and Future Work

To allow complete plastic tension field action to develop in the steel infill plates in all stories, it is required that the boundary frame members have a large inelastic deformation capacity. In the present

**Table 3.** Comparison of Analysis and Test Results

Specimens	Lateral-load-carrying capacity			Initial stiffness		
	$V_{exp}^a$ (kN)	$V_{pred}^b$ (kN)	$\frac{V_{pred}}{V_{exp}}^{a,b}$	$K_{exp}^a$ (kN/mm)	$K_{pred}^b$ (kN/mm)	$\frac{K_{pred}}{K_{exp}}^{a,b}$
SPIW1	886	739	0.83	53	50	0.94
SPIW2	914	800	0.88	55	52	0.95
RCF	190	173	0.91	6	6	1.00

<sup>a</sup>Test results.<sup>b</sup>Predictions (strip model).**Fig. 14.** Connection details between the columns and steel plates: (a) completely connected steel plate; (b) partially connected steel plate

study, to ensure the ductile behavior of the RCF, reinforcement details for the special moment frame (ACI 2008). were used. Thus, to achieve economical design, further study is required to develop the steel plate infilled walls that have an intermediate moment frame or an ordinary moment frame as the boundary frame.

To ensure the shear-dominated behavior shown in Fig. 1(a), columns should be designed to satisfy the requirements in Eqs. (1)–(3). When the strength of columns does not satisfy the requirements, the wall is expected to exhibit the flexure-dominated behavior, as shown in Fig. 1(b), or soft-story behavior. The ductility and energy dissipation of such walls are less than those of the walls showing shear-dominated behavior.

As shown in Fig. 7, the anchorage of the tension field force of the steel plates caused the formation of vertical concrete cracks that may result in unexpected column failure. To avoid such damage caused by cracks and the requirement of an excessive force from the tension field force of the steel plates, partially connected steel plates, as shown in Fig. 14(b), can be used. The partial connection was studied by Choi and Park (2009) for a steel moment frame with steel infill plates. By disconnecting the end plates of the steel infill panel from the column, the flexural moment and shear force transmitted to the column can be decreased. Thus, the strength requirements for the column decrease and the formation of vertical concrete cracks can be prevented. However, at the beam-column joints, the column should be connected to the steel plates to prevent premature failure at the beam-column joints. When such a partial connection is used, the effective area of the tension field decreases; and therefore, the tension field force of the steel plate decreases [see Fig. 14(b)]. In such a case, thicker end plates can be used to increase the tension field force. Although Choi and Park (2009) studied the structural performance of the steel plate walls with partial connections, experimental evidence is required to confirm the effect of the partial connection on the RCF with steel infill plates.

The details of the connection between the steel infill plates and the boundary frame that were used in this test were designed for

new construction. To apply the proposed method to existing RCFs, other connection details and the strengthening methods for columns need to be studied.

## Conclusions

An experimental study was performed to investigate the structural performance of a wall system that consists of a reinforced concrete boundary frame and thin steel infill plates, which were subjected to reverse cyclic loading. For comparison, a steel plate infilled wall with a wall opening, an RCIW, and an RCF were also tested. The test results showed that the displacement ductility and energy dissipation of the steel plate infilled walls were higher than those of the RCIW by factors of 2.3 and 3.5, respectively. The findings of the present experimental and numerical studies are summarized as follows:

1. Unlike RCIW, which exhibit cantilever flexure behavior, the steel plate infilled walls can be designed to exhibit ductile shear-dominated behavior by using thin steel plates. The test results demonstrated that by distributing the yielding of the steel infill plates along the wall height, the steel plate infilled walls can be made to have excellent deformation capacity as well as high strength.
2. Because of the strengthening effect provided by the steel infill plates, shear cracking at the beam-column joints in the reinforced concrete boundary frame was prevented.
3. In the columns and beams, longitudinal concrete cracks were developed because of the anchorage force transmitted by the tension field action in the steel infill plates. Therefore, in the design of columns, the anchorage forces should be carefully considered to avoid premature failure of the column and anchorage.
4. The strip model predicted the strength and initial stiffness of the steel plate infilled walls accurately.

## Acknowledgments

This research was financially supported by the Korean Ministry of Land, Transportation and Maritime Affairs (MLTM) through the High-tech Urban Development Program (HUDP) of the Korea Institute of Construction & Transportation Technology Evaluation and Planning (KICTEP); the authors are grateful to the authorities for their support.

## References

- American Concrete Institute (ACI). (2008). "Building code requirements for structural concrete and commentary." *ACI 318-08 and ACI 318R-08*, Farmington Hills, MI.
- Baldelli, J. A. (1983). "Steel shear walls for existing buildings." *Eng. J.*, 20(2), 70–77.
- Berman, J., and Bruneau, M. (2003). "Plastic analysis of steel plate shear walls." *J. Struct. Eng.*, 129(11), 1448–1456.
- Caccese, V., Elgaaly, M., and Chen, R. (1993). "Experimental study of thin steel-plate shear walls under cyclic load." *J. Struct. Eng.*, 119(2), 573–587.
- Choi, I. R., and Park, H. G. (2008). "Ductility and energy dissipation capacity of shear-dominated steel plate walls." *J. Struct. Eng.*, 134(9), 1495–1507.
- Choi, I. R., and Park, H. G. (2009). "Steel plate shear walls with various infill plate designs." *J. Struct. Eng.*, 135(7), 785–796.
- Driver, R. G., Kulak, G. L., Kennedy, D. J. L., and Elwi, A. E. (1998). "Cyclic test of a four-storey steel plate shear wall." *J. Struct. Eng.*, 124(2), 111–120.
- Elgaaly, M. (1998). "Thin steel plate shear walls behavior and analysis." *Thin-Walled Struct.*, 32, 151–180.
- Lubell, A. S., Prion, H. G. L., Ventura, C. E., and Rezai, M. (2000). "Unstiffened steel plate shear wall performance under cyclic loading." *J. Struct. Eng.*, 126(4), 453–460.
- Mazzoni, S., McKenna, F., Scott, M. H., and Fenves, G. L. (2006). "Open system for earthquake engineering simulation, user command-language manual, Version 1.7.3." *Pacific Earthquake Engineering Research Center*, Univ. of California, Berkeley, CA (<http://opensees.berkeley.edu/OpenSees/manuals/usermanual/index.html>).
- Park, H. G., Kwack, J. H., Jeon, S. W., Kim, W. K., and Choi, I. R. (2007). "Framed steel plate wall behavior under cyclic lateral loading." *J. Struct. Eng.*, 133(3), 378–388.
- Precast/Prestressed Concrete Institute (PCI). (1999). *PCI design handbook: Precast and prestressed concrete*, 5th Ed., Chicago.
- Thorburn, L. J., Kulak, G. L., and Montgomery, C. J. (1983). "Analysis and design of steel shear wall system." *Structural Engineering Rep. No. 107*, Dept. of Civil Engineering, Univ. of Alberta, Alberta, Canada.
- Timler, P. A., and Kulak, G. L. (1983). "Experimental study of steel plate shear walls." *Structural Engineering Rep. No. 114*, Dept. of Civil Engineering, Univ. of Alberta, Alberta, Canada.